IEEE Open Journal of the Communications Society

Received 25 August 2024; revised 10 September 2024; accepted 23 September 2024. Date of publication 25 September 2024; date of current version 3 October 2024.

Digital Object Identifier 10.1109/OJCOMS.2024.3467385

An LLR-Based Receiver for Mitigating Bursty Impulsive Noise With Unknown Distributions

HAZEM BARKA [1] (Graduate Student Member, IEEE), MD SAHABUL ALAM [2] (Senior Member, IEEE), GEORGES KADDOUM [1,3] (Senior Member, IEEE), MINH AU [4] (Member, IEEE), AND BASILE L. AGBA [4] (Senior Member, IEEE)

[1]Department of Electrical Engineering, ETS, Montreal, QC H3C 1K3, Canada

[2]Department of Electrical and Computer Engineering, California State University, Northridge, CA 91330, USA

[3]Artificial Intelligence and Cyber Systems Research Center, Department of Computer Science and Mathematics, Lebanese American University, Beirut 797751, Lebanon

[4]Hydro-Québec Research Institute (IREQ), Varennes, QC J3X 1S1, Canada

CORRESPONDING AUTHOR: H. BARKA (e-mail: hazem.barka.1@ens.etsmtl.ca)

ABSTRACT The rapid expansion of Internet of Things (IoT) networks has paved the way for their integration into mission-critical applications requiring secure and reliable monitoring, such as smart grid utilities. However, these advanced power grids face significant challenges in maintaining reliable wireless communication, particularly in hostile environments like high-voltage substations and power plants. These environments are characterized by intense bursts of interference, known as impulsive noise with memory. To address this problem, in this study, we introduce a two-process receiver design. The first process is a multi-step receiver parameter estimation process. The second process is a novel memory-aware log-likelihood ratio (LLR) calculation method designed to mitigate the effects of impulsive noise with memory using the parameters estimated from the first process. This method is computationally efficient, which makes it suitable for IoT devices with limited computational capabilities. Simulation results obtained show that the proposed method achieves a bit error rate (BER) similar to the corresponding BERs of the best-performing algorithms with perfect noise parameters. Furthermore, it outperforms the Viterbi algorithm amid imperfect noise parameters. Notably, it method achieves these benchmarks while substantially improving execution time.

INDEX TERMS Bursty impulsive noise, log-likelihood ratio, receiver design, machine learning, BCJR algorithm, Viterbi algorithm.

I. INTRODUCTION

THE INTERNET of Things (IoT) networks have grown rapidly during the past decade and started to be incorporated into several critical applications that require secure and reliable monitoring. For instance, several power producers are taking steps to modernize their grids by leveraging IoT networks for power substation and transmission line monitoring and control [1]. This approach not only enhances the efficiency and reliability of the grid but also helps to prevent potential blackouts and failures [1], [2], [3], [4]. Such incidents can result in serious risks for modern societies such as negative impacts on the economy, health and safety, etc. By implementing IoT-based solutions, power producers can mitigate these risks and ensure the safe and uninterrupted delivery of electricity to consumers. This example, and many others, are considered critical tasks without room for failure and highlight the importance of establishing robust wireless communications techniques for IoT devices.

These IoT-based solutions must consider radio frequency (RF) interference and realistic noise behavior in the designing process. In this vein, many noise level measurement campaigns have concluded that the additive white Gaussian noise (AWGN) assumption is far from reality in many environments, such as around high-voltage equipment [1], [3], [4], [5], [6], [7], [8], [9], [10], [11]. This type of equipment is nearly everywhere, from home and indoor appliances

TABLE 1. Summary of the LLR-based approaches for bursty impulsive noise mitigation in SC systems.

Method	Advantages	Drawbacks
Memoryless LLR approximation [17]–[23]	• Very simple and computationally efficient. • Acceptable BER for soft memoryless noise with low energy.	• The worst method in terms of BER, especially for impulsive noise with memory. • Challenging coefficients' estimation.
Memoryless exact LLR calculation [2], [18], [24]–[26]	• Optimal BER for memoryless impulsive noise. • Computationally efficient.	• The BER is unreliable for impulsive noise with a large memory in low SNR regimes. • Needs exact noise parameters.
Viterbi-based LLR calculation [27]–[29]	• Near-optimal BER performance.	• Computationally expensive. • Needs exact noise parameters.
BCJR-based LLR calculation [2], [30]–[34]	• Optimal BER performance.	• Very computationally expensive. • Needs exact noise parameters.
BNET-based LLR approximation [35]	• Near-optimal BER performance. • Computationally efficient.	• Works only in slow-fading environments. • Works only for TSMG noise scenarios. • Cannot be re-trained at the receiver.

(like microwaves, ovens, and printers) to power substation devices (such as circuit breakers and transformers). They are characterized as emitting impulsive noise, which refers to short and intense bursts of high-energy interference that can occur in the RF spectrum [1], [9], [10], [11].

Impulsive noise can be present in indoor and outdoor environments and will severely impact the performance of wireless communication systems. For example, it will cause errors in data transmission, disrupt signal quality, and lead to poor connections [1], [2], [3], [4], [7], [12], [13]. In some cases, impulsive noise can even cause permanent damage to wireless communication equipment [14]. Therefore, ensuring reliable wireless communication for IoT devices in the presence of impulsive noise is a crucial challenge that needs to be addressed, particularly for smart grids. In the majority of impulsive noise mitigation studies, single-carrier (SC) communication systems are preferred over orthogonal frequency-division multiplexing (OFDM)-based ones in IoT devices for two main reasons [2]. First, most IoT devices operate in low signal-to-noise ratio (SNR) regions, and SC modulation performs better than multicarrier modulation in the presence of impulsive noise at low SNR [15]. Second, SC modulation outperforms OFDM when impulses are frequent or intense [16]. Therefore, SC modulation is a better choice for reliable communication between IoT devices in impulsive noise environments.

A. RELATED WORK

Numerous studies, including [17], [18], [19], [20], [21], [22], [23], [24], [25], [26], have proposed various wireless receivers to mitigate the impact of impulsive noise on wireless communication systems. However, they are limited by their memoryless assumption, which assumes that all noise samples are independent. The time correlation between noise samples, also known as the memory effect, is a fundamental characteristic that divides noise models into two categories: memoryless models and models with memory. The latter are also known as bursty impulsive noise models [2], [35]. Moreover, as the degree of correlation increases, mitigating the noise's effect becomes increasingly challenging. Several studies [1], [2], [3], [36] have highlighted that, like the AWGN assumption, the memoryless impulsive noise assumption is also far from reality, especially around electric grid installations. Furthermore, the authors of [2] showed that memoryless receivers perform poorly in scenarios where impulsive noise has a memory.

To the best of our knowledge, systems with low-density parity-check (LDPC) coding combined with memory-aware log-likelihood ratio (LLR)-based decoding are the most effective methods for mitigating bursty impulsive noise, and they exhibit reliable bit error rate (BER) performance in low SNR regions. The principle behind their improved performance is based on three components:

1) An LDPC encoder that provides information redundancy in case a symbol is lost after being impaired by an impulse.
2) A memory-aware LLR calculation module that computes the LLR of each symbol by utilizing a sequence instead of the corresponding symbol to take advantage of the time correlation between noise samples and use it to improve performance. The amplitude of the LLR characterizes the reliability of the bit. Higher noise amplitudes correspond to lower LLR absolute values [2].
3) An LDPC decoder that takes advantage of the LLR values and the bit reliability information they provide and decodes the bits accordingly.

The same principle is followed in numerous works, such as [2], [30], [31], [32], and [34], where the memory-aware LLR calculation is performed using an adapted version of the maximum *a posteriori* (MAP) algorithm, which is also known as the Bahl, Cocke, Jelinek, and Raviv (BCJR) algorithm [37]. Table 1 summarizes the existing LLR-based impulsive noise mitigation techniques in SC communication

systems. Nevertheless, none of these mentioned techniques are optimized for IoT devices in real-life scenarios for several reasons:

- Firstly, memoryless receivers are unable to incorporate noise memory, which is essential for optimal and near-optimal BER performance [2], [35].
- Secondly, current memory-aware receivers are based on the BCJR algorithm and the Viterbi algorithm, which suffer from expensive time complexity because of their recursive operations. Therefore, they are unsuitable for IoT devices with low computational capabilities and minimal battery consumption [2], [35], and [32].
- Finally, noise is non-stationary in real-life scenarios, meaning that its distribution changes constantly due to a variety of environmental factors, such as the voltage of nearby electrical equipment and humidity levels [1]. Therefore, reliable noise parameter estimation methods must be incorporated for impulsive noise with memory to mitigate the effect of changing noise characteristics.

In light of considering these aspects, in [35], we proposed a neural network framework called BCJR-mimicking neural network (BNET) to approximate the output of the BCJR algorithm. However, that study was limited to a simple two-state Markov-Gaussian (TSMG) noise model that performed poorly in more complex noise environments.

B. CONTRIBUTIONS

To overcome the limitations of the approaches mentioned in Table 1, in this article, we consider a more practical impulsive noise model with a larger number of states and propose a robust and computationally efficient alternative to the BCJR and Viterbi algorithms that works with any bursty impulsive noise distribution. The paper's contributions are presented as follows:

1) We propose a novel memory-aware LLR calculation method to mitigate the harmful effects of bursty impulsive noise. It is based on noise state detection using a dedicated neural network. Simulation results demonstrate that the proposed method performs as well as the BCJR and the Viterbi algorithms in terms of BER when the noise parameters are perfectly known. Moreover, it outperforms the Viterbi algorithm in scenarios with bursty impulsive noise, where the noise parameters are imperfect and its behavior is complex, involving multiple noise states. This improvement is due to the neural network's ability to recognize patterns.
2) We optimize the LLR calculation process to minimize its time complexity. As a result, the proposed approach is significantly faster than the BCJR algorithm. For example, it can process a one-Mbit sequence 500 times faster. This computational efficiency is crucial for low-latency communication. We propose to optimize the neural network by using a memory quantification method to estimate the minimal number of neurons required and applying Gaussian mixture models (GMMs) to estimate the noise parameters. We then use the GMMs' predictions to train the neural network as detailed in Section IV.

TABLE 2. Notations used in the article.

Variable	Description
K	Sequence length
S	Number of noise states
M	Modulation order
$b_{n,k}$	nth source bit carried by the kth symbol
$c_{i,k}$	ith encoded bit carried by the kth symbol
x_k	Transmitted symbol at time k
y_k	Received symbol at time k
n_k	Noise term at time k
h_k	Fading channel coefficient at time k
T_c	Coherence time
$\mathbf{y^K}$	Sequence of received symbols
$\mathbf{n^K}$	Sequence of noise samples
$\mathbf{s^K}$	Sequence of noise states
$\mathcal{N}(.\|\mu,\sigma)$	Gaussian distribution probability density function (PDF) with mean μ and standard deviation σ
$\mathcal{N}(\mu,\sigma)$	Gaussian distribution with mean μ and standard deviation σ
σ_s^2	Variance of the Gaussian distribution for state s
$L_k^{(i)}$	LLR value for the ith bit at time k
$\mathbf{\Theta}$	Neural network parameters
$N_{\boldsymbol{I}}$	Input size to the neural network
$\boldsymbol{I_k}$	Preprocessed input vector for neural network at time k
γ_s^k	Probability that noise sample n_k belongs to state s
ξ	Noise memory parameter
$\boldsymbol{T}$	Transition matrix
ϵ_k	Channel state information (CSI) error at time k
σ_ϵ	Standard deviation of CSI error
$\hat{h}_k$	Estimated fading channel coefficient at time k
π_s	Steady-state probability of state s
N_s	Number of samples assigned to state s
$LL(S)$	Log-likelihood function for S states
B	Number of samples in the balanced dataset
δ	Convergence threshold
$u(.)$	Gradient-based optimizer function
$J(\mathbf{\Theta})$	Cross-entropy loss function
$AC(\|\mathbf{n^K}|,\tau)$	Autocorrelation function for noise amplitudes over time lag τ
$g(\xi)$	Function representing the sum of autocorrelatio n over noise memory parameter ξ
$O(.)$	Big O notation of time complexity
C_{proposed}	Time complexity of the proposed method
C_{Viterbi}	Time complexity of the Viterbi algorithm
C_{BCJR}	Time complexity of the BCJR algorithm

C. ORGANIZATION

The rest of the article is structured as follows: Section II introduces the system model and provides an overview of the noise model considered. In Section III, we delve into the methods that can be used to calculate the LLR in the presence of both memoryless and bursty impulsive noise. Additionally, we present the proposed receiver architecture in Section IV. In Section V, we discuss the computational advantages of using the proposed LLR calculation method. All the simulation results and interpretations are discussed in Section VI. Finally, we conclude the article in Section VII.

D. NOTATIONS

See Table 2.

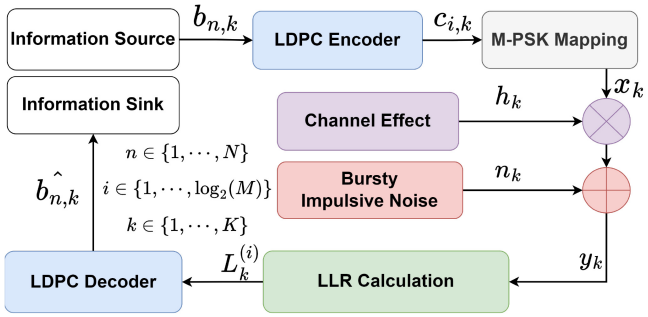

FIGURE 1. Block diagram of the system model considered for impulsive noise mitigation in an LDPC-coded M-PSK transmission scheme.

II. SYSTEM MODEL

The system model considered in this paper is represented in Fig. 1. It consists of an M-ary phase shift keying (M-PSK) modulated transmission that is LDPC-coded and affected by Rayleigh fading and impulsive noise with memory. An S-state Markov-Gaussian model is used to represent the noise.

A. SIGNAL MODEL

The signal received at each timestep $k \in \{1, \ldots, K\}$ is expressed as:

$$y_k = h_k x_k + n_k, \tag{1}$$

where x_k is the transmitted symbol, n_k is the noise term, and h_k is the fading channel coefficient modeled as a zero-mean, circularly symmetric complex Gaussian random variable with variance σ_h^2. It is assumed that h_k varies every T_c symbol. During the rest of the study, $\mathbf{y^K}$ and $\mathbf{n^K}$ refer to the sequences $(y_1, \ldots, y_K)$ and $(n_1, \ldots, n_K)$, respectively.

B. NOISE MODEL

The Markov-Gaussian noise model is a statistical representation that captures the dependencies of noise samples in a time series. Unlike white Gaussian noise, which is characterized as being independent and identically distributed (i.i.d.) across samples, Markov-Gaussian noise introduces a state-dependent correlation structure governed by a hidden Markov model (HMM). Therefore it can effectively replicate the bursty impulsive noise's behavior [2], [3], [27], [30], [35], [36], [38]. In this system model, the noise term n_k at each discrete time index k is a Gaussian random variable with state-dependent mean μ_s and variance σ_s^2. The subscript s denotes the current state of the Markov process, which can range from 1 to S, where S is the total number of states in the Markov model. Each state s is associated with a Gaussian distribution, which is denoted by $\mathcal{N}(\mu_s, \sigma_s)$, with mean μ_s and variance σ_s^2. The state transitions are governed by a stochastic matrix $\boldsymbol{T}$, where each element T_{ij} represents the probability of transitioning from state i to state j. To generate the noise sequence $\mathbf{n^K}$, we first generate a state sequence $\mathbf{s^K} = (s_1, .., s_K)$ using the transition probabilities, and then generate a noise sample n_k from $\mathcal{N}(n_k|\mu_s, \sigma_s)$ for each $s_k = s$.

III. LLR CALCULATION

A. LLR CALCULATION FOR MEMORYLESS IMPULSIVE NOISE

Assuming that we know h_k, the LLR value of $c_{i,k}$ (the ith encoded bit carried by the kth symbol) is calculated as follows:

$$L_k^{(i)} = \log\left\{\frac{p(c_{i,k} = 1 \mid y_k, h_k)}{p(c_{i,k} = 0 \mid y_k, h_k)}\right\} \tag{2}$$

$$= \log\left\{\frac{\sum_{x\in\chi(1)} p(x_k = x \mid y_k, h_k)}{\sum_{x\in\chi(0)} p(x_k = x \mid y_k, h_k)}\right\} \tag{3}$$

$$= \log\left\{\frac{\sum_{x\in\chi(1)} f_n(y_k - x \cdot h_k)}{\sum_{x\in\chi(0)} f_n(y_k - x \cdot h_k)}\right\}, \tag{4}$$

where f_n is the noise PDF, and $\chi(c) = \chi(c_{i,k} = c)$ is the set of all symbol hypotheses x that would result in the i-th encoded bit equaling $c \in \{0, 1\}$.

To obtain a closed-form expression of $L_k^{(i)}$, we need to find the closed-form expression of the noise PDF f_n. However, this is optimal only in some cases where the noise samples are assumed to be i.i.d. This assumption holds for the AWGN model and some memoryless impulsive noise models, such as Middleton Class A [18], [25], [26], and the memoryless Gaussian mixture (GM) model. For instance, the PDF of GM-modeled noise composed of S Gaussian distributions can be computed as:

$$f_{GM}(n) = \sum_{s=1}^{S} \pi_s \cdot \mathcal{N}(n \mid \mu_s, \sigma_s), \tag{5}$$

where

$$\sum_{s=1}^{S} \pi_s = 1 \quad \text{and} \quad \pi_s \geq 0 \quad \forall s \in \{1, \ldots, S\}.$$

It is worth mentioning that under the memoryless assumption, the Markov-Gaussian models are reduced to a GM model with π_s equals the steady-state probability of the state s (also called the stationary probability). Therefore, in this study, the memoryless LLR receiver refers to the following LLR calculation:

$$L_{GM,k}^{(i)} = \log\left\{\frac{\sum_{x\in\chi(1)} \sum_s \pi_s \cdot \mathcal{N}(y_k - x \cdot h_k \mid \mu_s, \sigma_s)}{\sum_{x\in\chi(0)} \sum_s \pi_s \cdot \mathcal{N}(y_k - x \cdot h_k \mid \mu_s, \sigma_s)}\right\}. \tag{6}$$

To summarize, relying on the closed-form PDF is known to achieve optimal BER performance when the noise is assumed to be memoryless, and its statistics are known. However, the authors of [2] demonstrate that assuming the same when the noise has a persistent memory leads to poor BER performance.

B. LLR CALCULATION FOR IMPULSIVE NOISE WITH MEMORY

To achieve optimal BER performance when impulsive noise exhibits memory, it is crucial to employ detection criteria that can handle the temporal dependencies within the noise,

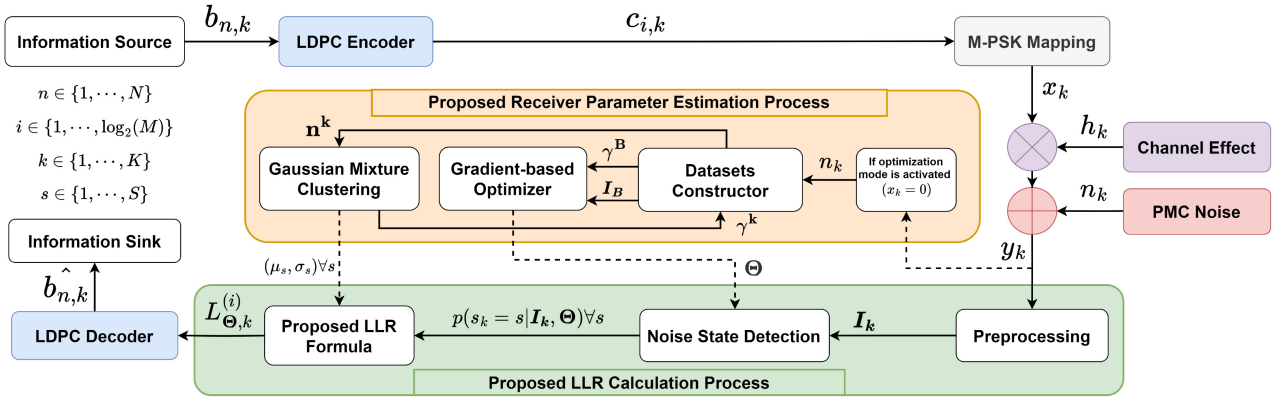

FIGURE 2. The receiver architecture proposed for bursty impulsive noise mitigation.

such as the MAP detection criterion used in the BCJR algorithm. In [2], the authors highlighted the optimality of the BCJR algorithm in tracking noise variations and calculating accurate LLR values. As outlined in [2], the BCJR algorithm calculates the *a posteriori* probabilities $p(x_k = x \mid y_k, h_k)\ \forall\ x$. Then, we get the LLRs using (3).

Conversely, the Viterbi algorithm, commonly used for its computational efficiency, estimates the noise state sequence $(\hat{s_1}, \hat{s_2}, \ldots, \hat{s_K})$ using the maximum likelihood estimation through a similar trellis representation [28]. This estimated sequence is then used to compute the LLRs, conditioned on $\hat{s_k}$, as follows:

$$L^{(i)}_{\text{Viterbi},k}(\hat{s_k}) = \log\left\{\frac{\sum_{x\in\chi(1)} p(x_k = x \mid y_k, h_k, \hat{s_k})}{\sum_{x\in\chi(0)} p(x_k = x \mid y_k, h_k, \hat{s_k})}\right\} \tag{7}$$

$$= \log\left\{\frac{\sum_{x\in\chi(1)} \mathcal{N}(y_k - x \cdot h_k \mid \mu_{\hat{s_k}}, \sigma_{\hat{s_k}})}{\sum_{x\in\chi(0)} \mathcal{N}(y_k - x \cdot h_k \mid \mu_{\hat{s_k}}, \sigma_{\hat{s_k}})}\right\}. \tag{8}$$

Although both the Viterbi and BCJR algorithms are integral to systems' ability to combat impulsive noise with memory, the Viterbi algorithm is frequently favored for its computational efficiency while the BCJR is a preferred option for its high precision. In addition, the BNET framework [35] is designed to approximate the BCJR algorithm's output. However, BNET works only in slow-fading environments and demonstrates poor performance in fast-fading scenarios and complex noise models.

C. LLR CALCULATION UNDER THE GENIE CONDITION: A LOWER BER BOUND

The genie condition assumes perfect knowledge of the noise state information (NSI) at each timestep k. In other words, we have precise information about the Gaussian distribution that the noise sample n_k belongs to. Therefore, the genie condition provides the LLRs that achieve the lower bound of the BER for any Markov-Gaussian noise model. Given the exact noise state s_k, the LLR is expressed as:

$$L^{(i)}_{\text{genie},k}(s_k) = \log\left\{\frac{\sum_{x\in\chi(1)} \mathcal{N}(y_k - x \cdot h_k \mid \mu_{s_k}, \sigma_{s_k})}{\sum_{x\in\chi(0)} \mathcal{N}(y_k - x \cdot h_k \mid \mu_{s_k}, \sigma_{s_k})}\right\}. \tag{9}$$

IV. THE PROPOSED LLR-BASED RECEIVER FOR IMPULSIVE NOISE WITH MEMORY

The proposed architecture is illustrated in Fig. 2 and comprises several parts. However, our main contribution is divided into two processes–the LLR calculation process and the receiver parameter estimation process–that are detailed in Sections IV-A and IV-B.

A. THE PROPOSED LLR CALCULATION PROCESS

In reality, having perfect knowledge of the NSI is impossible; therefore, the genie condition is used only for benchmarking purposes. We propose to approximate the genie condition using a new LLR calculation method based on the principle of determining the probability of each possible LLR value. We suggest using a neural network, illustrated by Fig. 3, to estimate the probabilities. The desired LLR value is then calculated by summing all possible LLR values multiplied by their respective probabilities. These possible LLR values are none other than the Gaussian LLR values conditioned on the noise state. Thus, the novel LLR formula can be expressed as follows:

$$L^{(i)}_{\Theta,k} = \sum_{s=1}^{S} p(s_k = s | \boldsymbol{I_k}, \Theta) \tag{10}$$

$$\times \log\left\{\frac{\sum_{x\in\chi(1)} \mathcal{N}(y_k - x \cdot h_k \mid \mu_s, \sigma_s)}{\sum_{x\in\chi(0)} \mathcal{N}(y_k - x \cdot h_k \mid \mu_s, \sigma_s)}\right\}, \tag{11}$$

where $p(s_k = s|\boldsymbol{I_k}, \Theta)$ denotes the probability that the noise sample n_k belongs to state s given a preprocessed input vector $\boldsymbol{I_k}$. The estimation of $p(s_k = s|\boldsymbol{I_k}, \Theta)$ requires a neural network and is done in four phases as detailed in Algorithm 1. First, for each y_k, we consider the input sequence $(y_{k-\xi//2}, \ldots, y_k, \ldots, y_{k+\xi//2})$, where ξ is the noise memory and quantifies the degree to which the impulses are correlated in time. Then we create a preprocessed vector $\boldsymbol{I_k}$ of size $N_I = 3 \times \xi + 1$, which consists of the essential components influenced by the noise (amplitude, real, and imaginary parts) of all symbols in the input sequence plus a bias term (also called offset). The input is then rescaled using normalization and forwarded to the neural network's

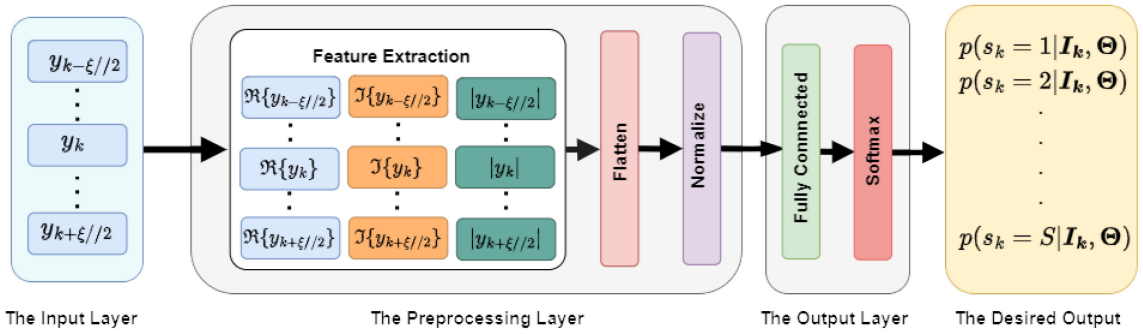

FIGURE 3. The light neural network architecture proposed for noise state detection. $\Re(.)$ and $\Im(.)$ denote the real and imaginary parts, respectively.

Algorithm 1 Summary of the Proposed LLR Calculation Process

Input: $\mathbf{y^K}$, $\boldsymbol{\Theta}$, γ, and $(\mu_s, \sigma_s)\forall s \in \{1, \ldots, S\}$.
Output: $L^{(i)}_{\boldsymbol{\Theta},k}$ $\forall i \in \{1, \ldots, \log_2(M)\}$ $\forall k \in \{1, \ldots, K\}$.
for y_k in $\mathbf{y^K}$ **do**

1. Prepare an input vector:

$$\boldsymbol{I_k} \leftarrow [1, |y_{k-\xi//2}|, \Re\{y_{k-\xi//2}\}, \Im\{y_{k-\xi//2}\}, .., |y_{k+\xi//2}|, \Re\{y_{k+\xi//2}\}, \Im\{y_{k+\xi//2}\}],$$

2. Rescale $\boldsymbol{I_k}$ using normalization.
3. Calculate $p(s_k = s|\boldsymbol{I_k}, \boldsymbol{\Theta})\forall s \in \{1, \ldots, S\}$ using:

$$p(s_k = s|\boldsymbol{I_k}, \boldsymbol{\Theta}) \leftarrow \frac{\exp(-\boldsymbol{\Theta}_s \cdot \boldsymbol{I_k})}{\sum_{j=1}^{S} \exp(-\boldsymbol{\Theta}_j \cdot \boldsymbol{I_k})},$$

where $\boldsymbol{\Theta}_s$ is the sth line of the matrix $\boldsymbol{\Theta}$.

4. Calculate $L^{(i)}_{\boldsymbol{\Theta},k}$ $\forall i \in \{1, \ldots, \log_2(M)\}$ using:

$$L^{(i)}_{\boldsymbol{\Theta},k} \leftarrow \sum_{s=1}^{S} p(s_k = s|\boldsymbol{I_k}, \boldsymbol{\Theta}) \times \log\left\{\frac{\sum_{x\in\chi(1)} \exp\left(-\frac{(y_k - x\cdot h_k - \mu_s)^2}{2\sigma_s^2}\right)}{\sum_{x\in\chi(0)} \exp\left(-\frac{(y_k - x\cdot h_k - \mu_s)^2}{2\sigma_s^2}\right)}\right\}.$$

end for

output layer, which has parameters $\boldsymbol{\Theta} \in \mathbb{R}^{S\times N_I}$. We refer to this neural network as the noise state detection model because its goal is to compute the probabilities $p(s_k = s|\boldsymbol{I_k}, \boldsymbol{\Theta})$ for all $s \in \{1, \ldots, S\}$ by performing S linear combinations in the form of $\boldsymbol{\Theta}_s\boldsymbol{I_k} = \sum_{i=1}^{N_I} \boldsymbol{\Theta}_{s,i} I_{k,i}$. The normalized exponential function (softmax) is then applied to these linear combinations to predict a multi-class probability distribution with $\sum_s p(s_k = s|\boldsymbol{I_k}, \boldsymbol{\Theta}) = 1$. This neural network architecture is selected to create a balance between accuracy and computational complexity. Finally, we calculate the LLRs using (10) and forward them to the LDPC decoder. It is worth mentioning that $L^{(i)}_{\boldsymbol{\Theta},k}$ converges to $L^{(i)}_{\text{genie},k}$ when $p(s_k = s|\boldsymbol{I_k}, \boldsymbol{\Theta})$ is accurately estimated.

Unlike other algorithms such as BCJR and Viterbi, the proposed LLR calculation process does not involve recursive and time-consuming loops. Instead, to calculate the LLRs, it uses short sequences of size γ, matrix multiplications, and element-wise operations. Accordingly, its execution time is much shorter than that of the other algorithms. The enhanced BER performance is attributed to the neural network-based pattern recognition ability and the receiver parameter estimation process, as detailed in the next subsection.

B. THE RECEIVER PARAMETER ESTIMATION PROCESS

To ensure the reliability of the proposed LLR calculation method, several parameters should be estimated. The parameter estimation process is summarized in Algorithm 2 and is only executed whenever a reduction in the desired quality of service (QoS) metric, such as the BER, is observed. The process consists of the following two steps. First, we estimate the impulsive noise parameters (the number of states S, (μ_s, σ_s) $\forall$ $s \in \{1, \ldots, S\}$, and the noise memory parameter, ξ). The second step consists of constructing a dataset and training the neural network (the noise state detection model) by iteratively updating $\boldsymbol{\Theta}$ using a gradient descent optimizer.

Step 1: Estimating the impulsive noise parameters (S, (μ_s, σ_s) $\forall$ $s \in \{1, \ldots, S\}$, and ξ): This operation can be challenging, especially for impulsive noise with memory. Furthermore, these parameters change over time. Therefore, an online parameter estimation technique is needed.

As a solution, we propose a clustering-based method that uses unsupervised GMMs. GMMs have a reputation for being universal approximators, given enough Gaussians [39]. As previously discussed, these Gaussians represent the noise states in the context of impulsive noise modeling. To estimate the parameters for each state, we have adopted an expectation-maximization (EM) algorithm [40], detailed in Algorithm 2. It involves clustering a noise sequence $\mathbf{n^K}$ and estimating the parameters (μ_s, σ_s) for each state s, as well as the probability of each noise sample n_k belonging to the state γ_s^k. A sample output from this operation is shown in Fig. 4, with the different colors indicating different noise states. The number of states S can be the subject of an optimization problem, in which we minimize the Bayesian information criterion (BIC):

$$S^* = \arg\min_S S \cdot \log(K) - 2\log(LL(S)), \tag{12}$$

Algorithm 2 The Receiver Parameter Estimation Process

Input: Captured noise sequence $\mathbf{n^K} = (n_1, n_2, \ldots, n_K)$, convergence threshold $\delta = 10^{-4}$, and the maximum number of noise states S_{max}.

Output: The optimal number of noise states S^* and parameters $(\mu_s, \sigma_s)\forall s \in \{1, \ldots, S^*\}$ in addition to the trained neural network parameters $\boldsymbol{\Theta}$.

I. First step: Noise parameters estimation
I.0. Initialize μ_s, σ_s, π_s, the log-likelihood LL and LL_{old}.
I.1. Estimate $(\mu_s, \sigma_s)\forall s$ using the EM algorithm:

for $S \in [2, S_{max}]$ **do**
  while $\mid LL(S) - LL_{old} \mid < \delta$ **do**
    for $k \in \{1, \ldots, K\}$ **do**

$$\gamma_s^k = p\Big(s_k = s \mid \mathbf{n^K}\Big) \leftarrow \frac{\pi_s \cdot \mathcal{N}(n_k \mid \mu_s, \sigma_s)}{\sum_{j=1}^{S} \pi_j \cdot \mathcal{N}\big(n_k \mid \mu_j, \sigma_j\big)}.$$

    end for
    for $s \in \{1, \ldots, S\}$ **do**

$$\mu_s \leftarrow \frac{1}{N_s} \sum_{k=1}^{K} \gamma_s^k n_k,$$
$$\sigma_s \leftarrow \frac{1}{N_s} \sum_{k=1}^{K} \gamma_s^k (n_k - \mu_s)(n_k - \mu_s)^T,$$
$$\pi_s \leftarrow \frac{N_s}{K}, \quad \text{with} \quad N_s = \sum_{k=1}^{K} \gamma_s^k.$$

    end for
    $LL_{old} \leftarrow LL(S)$

$$LL(S) \leftarrow \sum_{k=1}^{K} \log\Big(\sum_{s=1}^{S} \pi_s \mathcal{N}(n_k \mid \mu_s, \sigma_s)\Big).$$

  end while
end for

I.2. $S^* \leftarrow \underset{S}{\text{argmin}}(S \cdot \log(K) - 2\log(LL(S)))$.
I.3. Repeat the previous while loop using $S = S^*$ to get the final $(\mu_s, \sigma_s)\ \forall\ s \in \{1, \ldots, S\}$.
I.4. Estimate the noise memory parameter:

$$\xi^* \leftarrow \underset{\xi}{\text{argmin}}(\log(\xi) \cdot K \cdot \sigma^2_{|\mathbf{n^K}|} - \sum_{\tau=1}^{\xi} \sum_{k=\tau+1}^{K} (|n_k| - \mathbb{E}[|n_k|])(|n_{k-\tau}| - \mathbb{E}[|n_k|])).$$

II. Second step: Neural network training
II.1.Dataset generation process:

for $k \in \{1, \ldots, K\}$ **do**
  i. Generate a pair (x_k, h_k).
  ii. $y_k \leftarrow x_k \cdot h_k + n_k$.
  iii.

$$\boldsymbol{I_k} \leftarrow [1, |y_{k-\xi^*//2}|, \Re\{y_{k-\xi^*//2}\}, \Im\{y_{k-\xi^*//2}\}, .., |y_{k+\xi^*//2}|, \Re\{y_{k+\xi^*//2}\}, \Im\{y_{k+\xi^*//2}\}],$$

  iv. Normalize $\boldsymbol{I_k}$.
  v. $\gamma^k \leftarrow [\gamma_1^k, .., \gamma_S^k]$.
end for
II.2. Balance the dataset $(\boldsymbol{I_b}, \gamma^b)\forall b \in \{1, \ldots, B\}$ using under-sampling.
II.3. Optimize $\boldsymbol{\Theta}$:
while $\|\nabla J(\boldsymbol{\Theta})\| < \delta$ **do**

$$J(\boldsymbol{\Theta}) \leftarrow \sum_b \sum_s \gamma_s^b \cdot \log\left\{\frac{\exp(-\boldsymbol{\Theta}_s \cdot \boldsymbol{I_k})}{\sum_{j=1}^{S} \exp(-\boldsymbol{\Theta}_j \cdot \boldsymbol{I_k})}\right\},$$
$$\boldsymbol{\Theta} \leftarrow \boldsymbol{\Theta} - u(\nabla J(\boldsymbol{\Theta})),$$

where $u(.)$ depends on the optimizer and ∇ is the gradient operator.
end while

where LL is the log-likelihood function presented in Algorithm 2.

Now, we need to estimate the value of ξ. In our case, the optimal value of ξ allows for maximum average temporal correlation between the elements of the input sequence $(y_{k-\xi//2}, .., y_k, .., y_{k+\xi//2})$. To estimate ξ, we propose using the autocorrelation function $AC(|\mathbf{n^K}|, \tau)$, which characterizes the degree of correlation between the noise amplitudes of the sequence $\mathbf{n^K}$ over a time lag τ. AC is given by:

$$AC(|\mathbf{n^K}|, \tau) = \frac{\sum_{k=\tau+1}^{K} (|n_k| - \mathbb{E}[|n_k|])(|n_{k-\tau}| - \mathbb{E}[|n_k|])}{\sum_{k=1}^{K} (|n_k| - \mathbb{E}[|n_k|])^2}, \tag{13}$$

where $\mathbb{E}[|n_k|] = \frac{1}{K} \sum_{k=1}^{K} |n_k|$ is the expectation value of $|n_k|$. As the noise samples follow a Markov process, the temporal correlation between them–and consequently, the AC function–decreases as the time lag between them increases. Thus, we deduce and observe that the function $g(\xi) = \sum_{\tau=1}^{\xi} AC(|\mathbf{n^K}|, \tau)$ increases logarithmically with respect to ξ. Therefore, we can propose an objective function to determine the optimal value of ξ that maximizes g.

The penalizing term must contain a logarithm of ξ because g behaves logarithmically. Hence, the optimal value of ξ is given by:

$$\xi^* = \underset{\xi}{\text{argmin}}(\log(\xi) - g(\xi)) \tag{14}$$

$$= \underset{\xi}{\text{argmin}}(\log(\xi) - \sum_{\tau=1}^{\xi} AC(|\mathbf{n^K}|, \tau)) \tag{15}$$

$$= \underset{\xi}{\text{argmin}}\Bigg(\log(\xi) - \sum_{\tau=1}^{\xi} \frac{\sum_{k=\tau+1}^{K} (|n_k| - \mathbb{E}[|n_k|])(|n_{k-\tau}| - \mathbb{E}[|n_k|])}{\sum_{k=1}^{K} (|n_k| - \mathbb{E}[|n_k|])^2}\Bigg) \tag{16}$$

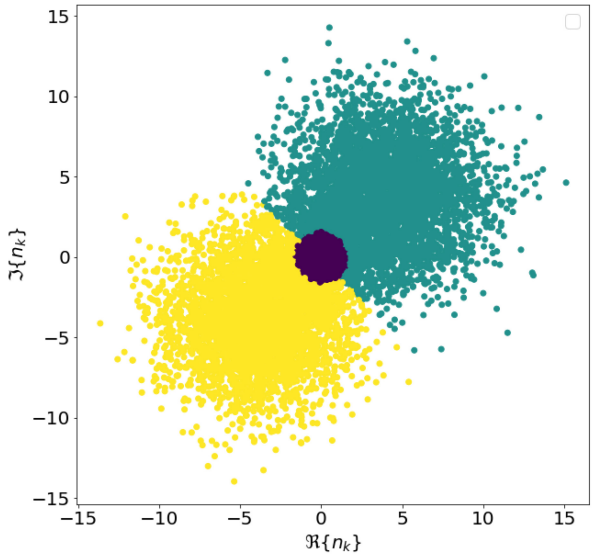

FIGURE 4. Illustration of the noise samples after clustering where every color corresponds to a noise state.

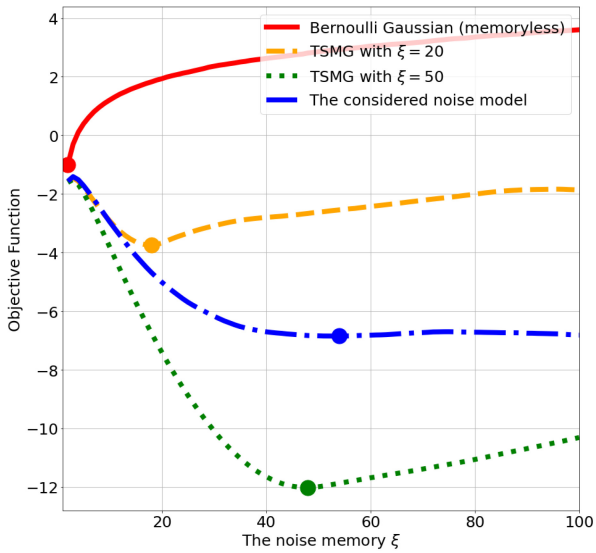

FIGURE 5. Estimation performance of the noise memory ξ.

$$= \underset{\xi}{\operatorname{argmin}} \Bigg(\log(\xi) \cdot K \cdot \sigma^2_{|\mathbf{n}^{\mathbf{K}}|} - \sum_{\tau=1}^{\xi} \sum_{k=\tau+1}^{K} (|n_k| - \mathbb{E}[|n_k|])(|n_{k-\tau}| - \mathbb{E}[|n_k|]) \Bigg), \quad (17)$$

where $\sigma^2_{|\mathbf{n}^{\mathbf{K}}|}$ represents the variance of the noise amplitudes. As shown in Fig. 5, this method provides accurate estimations of ξ. The results are further validated by the simple and popular TSMG model for which the value of noise memory ξ is well known. Details about the TSMG model can be found in [2] and [35].

Step 2: Estimating the neural network's parameters $\boldsymbol{\Theta}$*:* The size of the matrix $\boldsymbol{\Theta}$ depends on the noise scenario. Specifically, $\boldsymbol{\Theta} \in \mathbb{R}^{S^* \times N_I^*}$, where $N_I^* = 3\xi^* + 1$, S^* is the optimal number of noise states, and ξ^* is the optimal noise memory value obtained using the proposed noise memory quantification method.

After the size of $\boldsymbol{\Theta}$ has been estimated, we optimize its elements. To do so, we begin by constructing a balanced dataset of $(\boldsymbol{I_b}, \gamma^b)$ for $b \in \{1, \ldots, B\}$, where the balance is obtained by having the same number of samples for each noise state. Next, we utilize this dataset to train the noise state detection model that estimates $\gamma_s^b = p(s_b = s \mid \boldsymbol{I_b}, \boldsymbol{\Theta})$ using a gradient-based optimizer, which minimizes the cross-entropy loss function $J(\boldsymbol{\Theta})$. The fact that the dataset is balanced ensures that the model is trained on an equal number of samples for each noise state, thereby preventing bias towards a particular state.

V. COMPUTATIONAL COMPLEXITY DISCUSSION

To comprehensively address the computational complexity of the proposed ANN-based LLR calculation method compared to the BCJR and the Viterbi algorithms, we derive the time complexity as a function of the number of noise states (S), modulation order (M), and sequence length (K). To this end, we manually calculated the number of operations required by each algorithm. The dominant terms in the simplified time complexities in terms of required operation are expressed as follows:

1) $C_{\text{proposed}} = O(K \cdot S \cdot M)$, showing a linear increase in complexity concerning the sequence length (K), the modulation order (M), and the number of noise states (S). This linear scaling implies that the method is highly efficient and scalable. This characteristic is particularly beneficial for systems with long sequences and multiple noise states, where computational resources may be limited.
2) $C_{\text{Viterbi}} = O(K \cdot M \cdot S + K \cdot S^2)$, reflecting a quadratic growth with the number of states. This arises from the need to evaluate and store path metrics for all state transitions. Each state transition involves computations dependent on both the modulation order (M) and the number of noise states (S), leading to a significant computational burden when S is large.
3) $C_{\text{BCJR}} = O(K \cdot M \cdot S^2)$, indicating that the complexity scales quadratically with the number of states. The BCJR algorithm requires more operations than the Viterbi algorithm, primarily due to the necessity of performing both forward and backward passes to compute state probabilities. This high complexity makes the BCJR algorithm the most computationally demanding among the three, posing challenges for real-time implementation in systems with numerous noise states and complex modulation schemes.

Fig. 6 shows a detailed visual comparison. It illustrates that while computational demands for Viterbi and BCJR significantly scale with increasing S and K, the proposed method maintains a lower and more stable operational footprint. This makes it a more efficient alternative, particularly

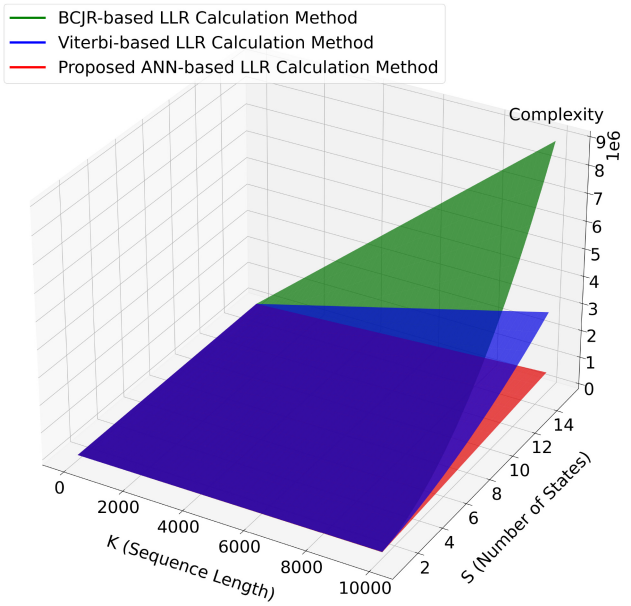

FIGURE 6. Computational efficiency comparison of the proposed method against the Viterbi and BCJR algorithms as functions of K and S for fixed $M = 4$.

attractive for modern communication systems requiring real-time processing and efficient resource utilization.

VI. SIMULATION RESULTS

In this section, we present the simulation results of the proposed LLR-based receiver and compare them with the other methods discussed in Section III. We assume that the channel coefficient varies every T_c symbols, and we have perfect knowledge of the channel state information (CSI). Note that the proposed method can work for any value of T_c. For LDPC coding, we use the fifth-generation (5G) standard with a code rate of 1/2 implemented using the Sionna framework [41] in Python. We set the number of iterations for decoding to 50, and we average the error rate over 100 frames, each containing 40,000 symbols, to obtain the BER performance values. The noise model's parameters are initialized based on the measurements campaign documented in [1], [8], and [36]. The remaining simulation parameters, such as the initialization method of $\boldsymbol{\Theta}$, size of the training dataset, learning rate, and optimizer, were selected based on their performance in minimizing the cross-entropy loss during neural network training (see Table 3). We use the standard implementation of the BCJR algorithm, which is presented in [2], and the Viterbi algorithm, which is presented in [42].

A. BER PERFORMANCE COMPARISON CONSIDERING PERFECT KNOWLEDGE OF THE NOISE PARAMETERS

The results of LDPC-coded quadrature phase shift keying (QPSK)-modulated transmission in the noise scenario considered and Rayleigh fading are presented in Fig. 7. We used extensive simulation to demonstrate that the proposed method is equally as reliable as the BCJR algorithm and

TABLE 3. The simulation settings.

Simulation parameter			Value
Noise model parameters	Variances $[(\text{mV})^2]$	σ_1^2	1
		σ_2^2	50
		σ_3^2	50
		σ_4^2	20
	Means [(mV)]	μ_1	0
		μ_2	5+5j
		μ_3	-5-5j
		μ_4	3+3j
	Transition matrix $\boldsymbol{T}$		$\begin{bmatrix} 0.995 & 0.005 & 0 & 0 \\ 0 & 0.8 & 0.2 & 0 \\ 0 & 0 & 0.8 & 0.2 \\ 0.3 & 0.4 & 0 & 0.3 \end{bmatrix}$
LDPC settings	LDPC matrix size		(4000, 8000)
	Number of LDPC decoding iterations		50
Neural network parameters	Optimal number of classes (or states) S^*		3
	Optimal memory parameter ξ^*		54
	$\boldsymbol{\Theta}$ initialization method		Normal distribution
	Size of training dataset B		80,000
	Learning rate		0.001
	Optimizer		Adam
	Number of training epochs		30
BER simulation settings	Number of frames for each SNR value		100
	Frame length [symbols]		40,000
Fading model parameter	Coherence time T_c [symbols]		10

the Viterbi algorithm, which are renowned for their optimal and near-optimal performance, respectively. The fact that the method performs as well as these well-established algorithms substantiates its potential as a viable alternative in practical communication systems. This is particularly noteworthy given that both reference algorithms have been shown to closely approach the genie condition representing a theoretical performance lower bound, which assumes perfect knowledge of the noise state information. This result is indicative of efficient channel information utilization, which is crucial for high data rates and reliability in modern communication systems.

Additionally, the empirical evidence presented in Fig. 7 underscores the limitations of the memoryless noise assumption, which states that successive noise samples are i.i.d.

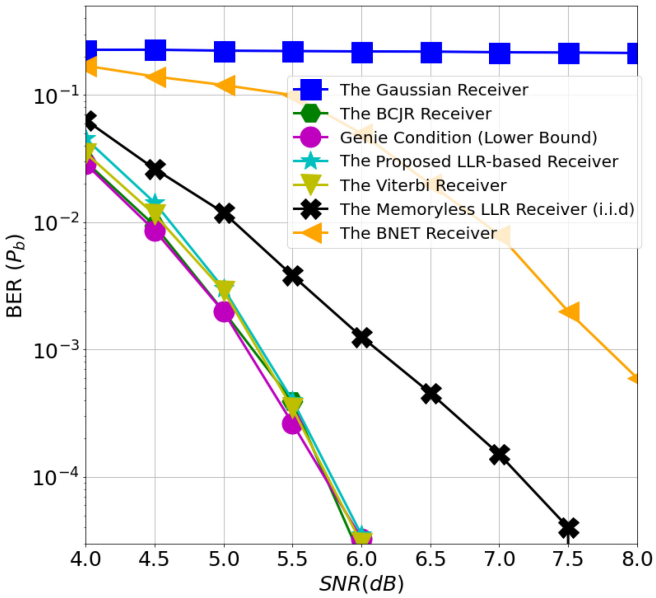

FIGURE 7. BER performance comparison for an LDPC-coded transmission employing QPSK modulation. We assume that we have perfect knowledge of the noise parameters.

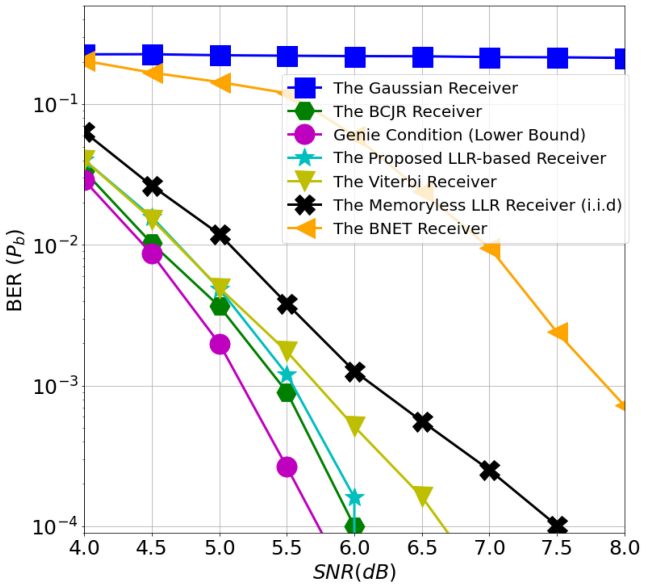

FIGURE 8. BER performance comparison for an LDPC-coded transmission employing QPSK modulation. The noise parameters are obtained using the EM algorithm presented in Algorithm 2.

These results contest this commonly adopted simplification and highlight its suboptimality and the need for memory-aware LLR calculation techniques for more accurate decoding.

Furthermore, the analysis presented also evaluates other receivers, such as the BNET and Gaussian receivers, with Markov-Gaussian noise models. When the BNET and Gaussian receivers are used with noise models that have more than two states, they exhibit a pronounced decline in reliability, as evidenced by their elevated BER in Fig. 7. This finding is critical, as it delineates the limit of these receivers' applicability and cautions against using them in scenarios where the noise model exhibits memory and has multiple states. It is worth noting that for SNR values below 4 *dB*, it is not feasible for any of the tested methods–including the BCJR receiver, Viterbi receiver, and the proposed receiver–to be reliable using QPSK modulation due to the combined effect of impulsive noise and Rayleigh fading.

B. BER PERFORMANCE COMPARISON WITHOUT THE KNOWLEDGE OF THE NOISE PARAMETERS

In practical communication scenarios, exact noise characteristics cannot be accurately measured. We address this challenge by adopting a probabilistic approach using a GMM to estimate the noise parameters, as detailed in Algorithm 2. Implementing this algorithm was both computationally feasible and efficient as it required only about one minute on an Intel® Core™ i7-11800H CPU. This rapid estimation process meets the needs of real-time communication systems, where the speed of adaptation to changing conditions is critical.

Fig. 8 shows the BER performance of various receivers under these estimated noise conditions. This figure's results lead to several important observations:

1) The BCJR receiver maintains its optimal performance even with the estimated noise parameters. This resilience to parameter imperfections suggests that the BCJR algorithm's inherent design can inherently withstand uncertainty in the noise model, which is a desirable trait in fluctuating communication environments.
2) the proposed neural network-based method is better able to exploit noise behavior patterns than the Viterbi receiver. Applying neural network techniques introduces a pattern recognition component that traditional statistical models lack. This advantage enables the proposed method to achieve a lower BER by compensating for the imperfect noise modeling, whereas the Viterbi algorithm's structure is limited in this regard.

Our method's performance advantage over the Viterbi receiver is indicative of the benefits that may be made possible by integrating machine learning methodologies into receiver design. This integration could enhance receivers' capability to adapt to and interpret complex noise patterns in the absence of perfect knowledge of the noise parameters, which is common in real-world communication channels.

C. EFFECT OF IMPERFECT CSI

Accurate CSI is pivotal for optimal receiver operation. To quantify the impact of inaccurate CSI, we modeled CSI error as a Gaussian perturbation added to the perfect CSI, which is expressed as $\hat{h}_k = h_k + \epsilon_k$, with $\epsilon_k \sim \mathcal{N}(0, \sigma_\epsilon)$ representing the error term. This model captures the practical scenario in which the channel estimation process is prone to error

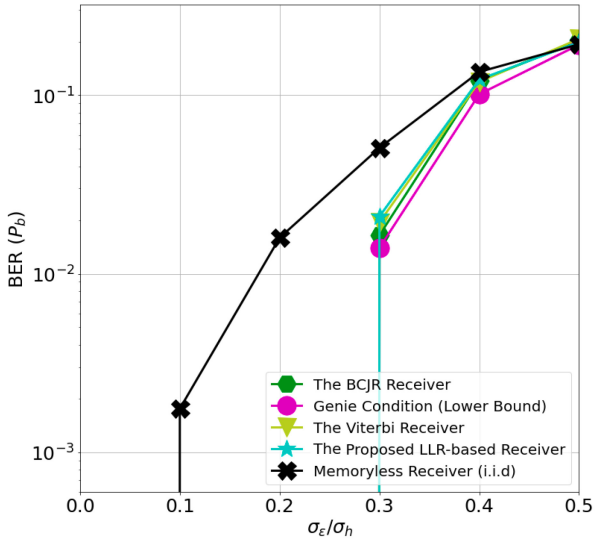

FIGURE 9. Illustration of the effect of imperfect CSI. We consider exact noise parameters, and the SNR = 8 *dB*.

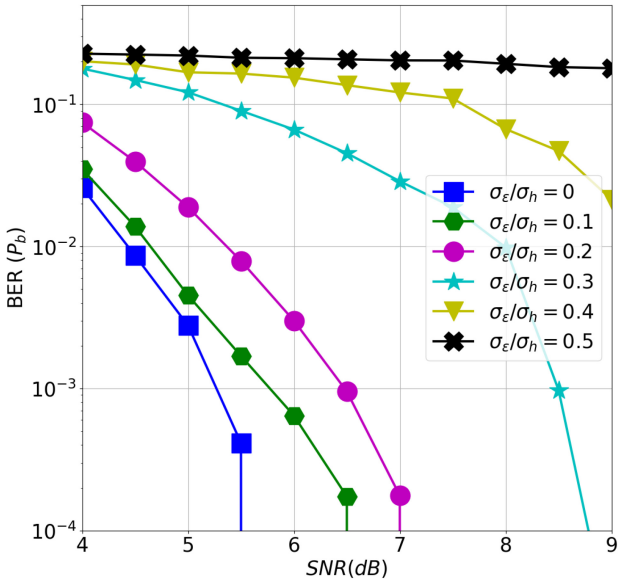

FIGURE 10. Illustration of the effect of imperfect CSI on BER performance for an LDPC-coded transmission employing QPSK modulation using the proposed LLR calculation process. The receiver is assumed to have perfect knowledge of the noise parameters.

and reflects a realistic and challenging condition for receiver performance.

We evaluated the robustness of the top four receivers–the proposed receiver, the BCJR receiver, the Viterbi receiver, and the memoryless receiver–in terms of BER with an SNR of 8 *dB*, as depicted in Fig. 9. The analysis revealed that the top three receivers are commendably tolerant to imperfect CSI, closely matching the genie condition up to a margin of $\frac{\sigma_\epsilon}{\sigma_h} = 0.3$. This level of tolerance indicates that these receivers are resilient and capable of compensating for a certain amount of CSI inaccuracy without substantial performance loss. This resilience is particularly crucial in environments where perfect CSI acquisition is challenging or infeasible.

In contrast, the memoryless receiver was highly sensitive to CSI imperfections, and its performance remained within acceptable bounds only when the error margin was limited to $\frac{\sigma_\epsilon}{\sigma_h} = 0.1$. This heightened sensitivity underscores the receiver's limitations in scenarios where a better channel state cannot be estimated.

Fig. 10 illustrates the impact of imperfect CSI on the BER performance of the proposed LLR calculation process against different SNR values. As shown in Fig. 10, in the perfect CSI scenario where $\sigma_\epsilon/\sigma_h = 0$, the system achieves the best performance. For $\sigma_\epsilon/\sigma_h < 0.3$, the system maintains acceptable BER performance, particularly in lower SNR regimes. However, when $\sigma_\epsilon/\sigma_h \geq 0.3$, a significant increase in transmit power is needed to reduce the impact of impulsive noise and, therefore, compensate for inaccurate CSI estimation.

D. EFFECT OF THE NUMBER OF STATES ON BER PERFORMANCE

Fig. 11 shows the impact of varying the considered number of states S in the EM algorithm used in Algorithm 2. Although the original noise model consists of four states,

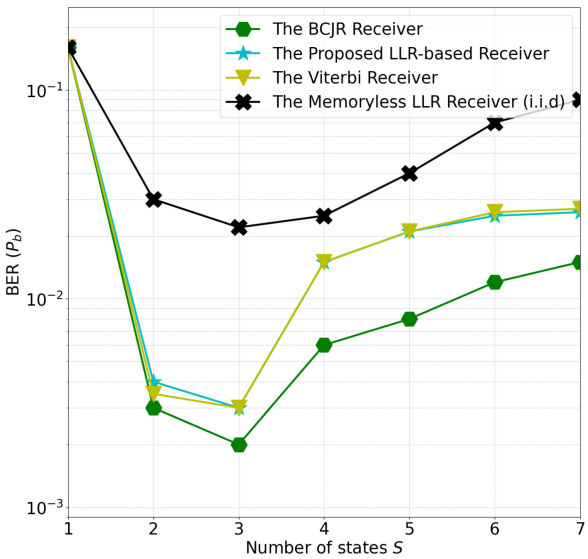

FIGURE 11. Illustration of the impact of the considered number of states on BER performance for an LDPC-coded transmission employing QPSK modulation using the proposed LLR calculation process. The noise parameters are obtained using the EM algorithm presented in Algorithm 2; the SNR = 5 *dB*.

Fig. 11 shows that the optimal number of states is three for all considered receivers. This outcome can be attributed to the overlap among the distributions of the different noise states (states s_2 and s_4), making it challenging to accurately and precisely estimate all four original states. Nevertheless, Algorithm 2 efficiently approximates the best number of states–three in this case–without directly calculating any BER, relying solely on the BIC criterion represented by Eq. (12) in Section IV. By identifying the most statistically significant number of states to provide the best BER

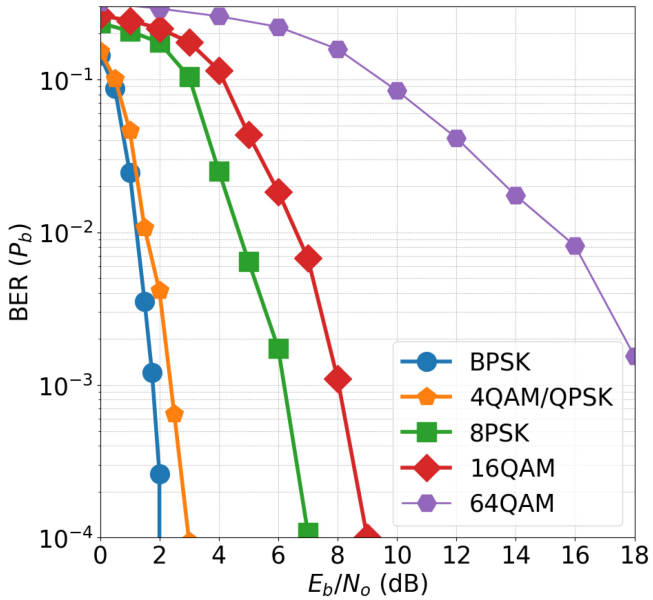

FIGURE 12. BER performance comparison of different modulation orders for an LDPC-coded transmission using the proposed LLR calculation process. The noise parameters are assumed to be known.

TABLE 4. A comparison of the top three LLR calculation methods in terms of average execution time for a one-Mbit sequence.

Method	Average execution time (in seconds)
The BCJR Receiver	523
The Viterbi Receiver	162
The Proposed LLR Receiver	1.7

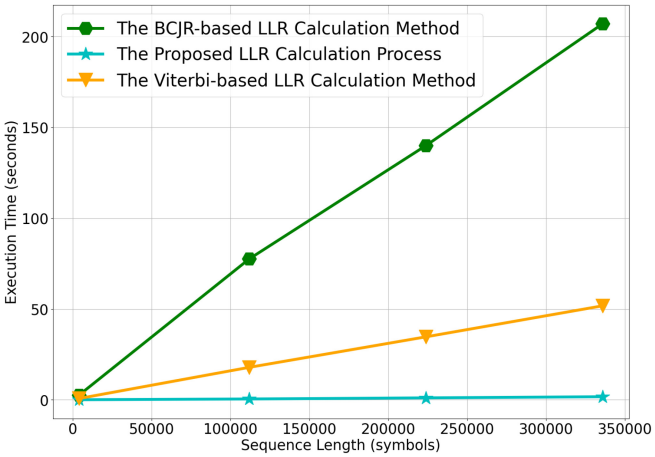

FIGURE 13. A comparison of the top three LLR calculation methods in terms of average execution time versus sequence length using NumPy.

performance, this approach underscores the utility of the BIC criterion and facilitates a more robust receiver design.

E. EFFECT OF THE MODULATION ORDER ON BER PERFORMANCE

In Fig. 12, we plot the BER performance for different modulation schemes against the energy per bit to noise power spectral density ratio (E_b/N_o) in *dB*. The modulation schemes tested include Binary Phase Shift Keying (BPSK), QPSK, 8PSK, 16-Quadrature Amplitude Modulation (16QAM), and 64QAM. Notably, the proposed receiver consistently demonstrates the capability to effectively manage and maintain reliable BER levels, which shows its versatility and flexibility and makes it suitable for diverse communication scenarios and requirements.

F. EXECUTION TIME COMPARISON

In this subsection, we conducted a comparative study to compare the average execution time of the top three methods, as shown in Table 4 and Fig. 13. We measured how long it took to calculate the LLR for a one-Mbit LDPC-coded and QPSK-modulated sequence. The tests were run on a single core of an Intel Core i7-11800H CPU using the Python programming language and the scikit-learn library for the simulation environment.

As indicated by Fig. 13, the proposed LLR receiver required substantially less execution time than the BCJR and Viterbi receivers. While the Viterbi receiver's execution time was moderate, the proposed receiver set a new benchmark with an average execution time of just 1.7 seconds for the one-Mbit sequence. This is a marked improvement over the Viterbi receiver's 162 seconds and the BCJR receiver's 523 seconds.

This drastic reduction in execution time is crucial. In the era of 5G and beyond, where latency is vital, a receiver's ability to quickly process signals can make the difference between a seamless user experience and a noticeable delay. Low-latency LLR calculation enables faster data processing, which is essential for upholding the stringent latency requirements of emerging communication protocols.

VII. CONCLUSION

In this article, we have addressed the critical challenge of ensuring reliable wireless communication for IoT devices in the presence of bursty impulsive noise. To this end, we proposed a multi-process receiver architecture. The study's contribution comprises a new computationally efficient LLR calculation process and a multi-step receiver parameter estimation process to enhance the performance amid non-stationary bursty impulsive noise.

The results of extensive simulations confirmed that, in terms of BER, the proposed LLR calculation method has a similar performance as compared to that of the BCJR and Viterbi algorithms, especially in scenarios with imperfect noise parameters where the proposed approach outperforms the Viterbi algorithm. Furthermore, the proposed approach significantly reduces the computational complexity, making it suitable for IoT devices with limited computational capabilities and minimal battery consumption.

In future research, we aim to investigate and mitigate the effects of this type of noise on the performance of OFDM and NOMA systems.

REFERENCES

[1] B. L. Agba, F. Sacuto, M. Au, F. Labeau, and F. Gagnon, *Impulsive Noise Measurements*. Cham, Switzerland: Springer Int. Publ., 2019, pp. 35–68. [Online]. Available: https://doi.org/10.1007/978-3-319-91328-5_3

[2] M. S. Alam, B. Selim, G. Kaddoum, and B. L. Agba, "Mitigation techniques for impulsive noise with memory modeled by a two state Markov-Gaussian process," *IEEE Syst. J.*, vol. 14, no. 3, pp. 4079–4088, Sep. 2020.

[3] F. Sacuto, F. Labeau, and B. L. Agba, "Wide band time-correlated model for wireless communications under impulsive noise within power substation," *IEEE Trans. Wireless Commun.*, vol. 13, no. 3, pp. 1449–1461, Mar. 2014.

[4] M. Zimmermann and K. Dostert, "Analysis and modeling of impulsive noise in broad-band powerline communications," *IEEE Trans. Electromagn. Compat.*, vol. 44, no. 1, pp. 249–258, Feb. 2002.

[5] I. Landa, M. Vélez, and A. Arrinda, "Impulsive noise measurements from consumer electronic devices," in *Proc. IEEE Conf. Antenna Meas. Appl. (CAMA)*, 2018, pp. 1–4.

[6] I. Landa, A. Blázquez, M. Vélez, and A. Arrinda, "Indoor measurements of IoT wireless systems interfered by impulsive noise from fluorescent lamps," in *Proc. 11th Eur. Conf. Antennas Propag. (EUCAP)*, 2017, pp. 2080–2083.

[7] K. Blackard, T. Rappaport, and C. Bostian, "Measurements and models of radio frequency impulsive noise for indoor wireless communications," *IEEE J. Sel. Areas Commun.*, vol. 11, no. 7, pp. 991–1001, Sep. 1993.

[8] M. Au, B. L. Agba, and F. Gagnon, "A model of electromagnetic interferences induced by corona discharges for wireless channels in substation environments," *IEEE Trans. Electromagn. Compat.*, vol. 57, no. 3, pp. 522–531, Jun. 2015.

[9] A. Mathur, M. R. Bhatnagar, and B. K. Panigrahi, "Performance evaluation of PLC under the combined effect of background and impulsive noises," *IEEE Commun. Lett.*, vol. 19, no. 7, pp. 1117–1120, Jul. 2015.

[10] A. Mathur, M. R. Bhatnagar, and B. K. Panigrahi, "On improving communication robustness in PLC systems for more reliable smart grid applications," *IEEE Trans. Smart Grid*, vol. 6, no. 6, pp. 2746–2756, Jul. 2015.

[11] J. Lin, M. Nassar, and B. L. Evans, "Impulsive noise mitigation in powerline communications using sparse Bayesian learning," *IEEE J. Sel. Areas Commun.*, vol. 31, no. 7, pp. 1172–1183, Jul. 2013.

[12] M. O. Asiyo and T. J. O. Afullo, "Analysis of bursty impulsive noise in low-voltage indoor power line communication channels: Local scaling behaviour," *SAIEE Afr. Res. J.*, vol. 108, no. 3, pp. 98–107, Sep. 2017.

[13] T. Bai et al., "Discrete multi-tone digital subscriber loop performance in the face of impulsive noise," *IEEE Access*, vol. 5, pp. 10478–10495, 2017.

[14] B. L. Agba, F. Sacuto, M. Au, F. Labeau, and F. Gagnon, *EMI and Wireless Communications in Power Substations*. Cham, Switzerland: Springer Int. Publ., 2019, pp. 7–33. [Online]. Available: https://doi.org/10.1007/978-3-319-91328-5_2

[15] T. Shongwe, A. J. H. Vinck, and H. C. Ferreira, "A study on impulse noise and its models," *SAIEE Afr. Res. J.*, vol. 106, no. 3, pp. 119–131, Sep. 2015.

[16] M. Ghosh, "Analysis of the effect of impulse noise on multicarrier and single carrier QAM systems," *IEEE Trans. Commun.*, vol. 44, no. 2, pp. 145–147, Feb. 1996.

[17] V. Dimanche, A. Goupil, L. Clavier, and G. Gelle, "On detection method for soft iterative decoding in the presence of impulsive interference," *IEEE Commun. Lett.*, vol. 18, no. 6, pp. 945–948, Jun. 2014.

[18] T. S. Saleh, I. Marsland, and M. El-Tanany, "A simplified LLR-based detector for signals in class-a noise," in *Proc. IEEE Veh. Technol. Conf.*, 2012, pp. 1–4.

[19] Y. Mestrah, A. Savard, A. Goupil, G. Gellé, and L. Clavier, "An unsupervised LLR estimation with unknown noise distribution," *EURASIP J. Wireless Commun. Netw.*, vol. 2020, no. 1, p. 26, Jan. 2020. [Online]. Available: https://doi.org/10.1186/s13638-019-1608-9

[20] L. Clavier, G. W. Peters, F. Septier, and I. Nevat, "Impulsive noise modeling and robust receiver design," *EURASIP J. Wireless Commun. Netw.*, vol. 2021, no. 1, p. 13, Jan. 2021. [Online]. Available: https://doi.org/10.1186/s13638-020-01868-1

[21] V. Dimanche, A. Goupil, L. Clavier, and G. Gellé, "Estimation of an approximated likelihood ratio for iterative decoding in impulsive environment," in *Proc. IEEE Wireless Commun. Netw. Conf.*, 2016, pp. 1–6.

[22] Y. Hou, R. Liu, and L. Zhao, "A non-linear LLR approximation for LDPC decoding over impulsive noise channels," in *Proc. IEEE/CIC Int. Conf. Commun. China (ICCC)*, 2014, pp. 86–90.

[23] Y. Mestrah et al., "Unsupervised log-likelihood ratio estimation for short packets in impulsive noise," in *Proc. IEEE Wireless Commun. Netw. Conf. (WCNC)*, 2022, pp. 944–949.

[24] K. Hägglund and E. Axell, "Adaptive demodulation in impulse noise channels," *IEEE Trans. Veh. Technol.*, vol. 71, no. 2, pp. 1685–1698, Feb. 2022.

[25] M. S. Alam, B. Selim, and G. Kaddoum, "Analysis and comparison of several mitigation techniques for Middleton class-a noise," in *Proc. IEEE Latin-Amer. Conf. Commun. (LATINCOM)*, 2019, pp. 1–6.

[26] T. Saleh, "Receiver design for signals in non-Gaussian noise: Applications to symmetric alpha-stable and Middleton's class-a noise models," Ph.D. dissertation, Dept. Syst. Comput. Eng., Carleton Univ., Ottawa, ON, Canada, 2012.

[27] F. G. Mengistu, D.-F. Tseng, Y. S. Han, M. A. Mulatu, and L.-C. Chang, "A robust decoding scheme for convolutionally coded transmission through a Markov gaussian channel," *IEEE Trans. Veh. Technol.*, vol. 63, no. 9, pp. 4344–4356, Nov. 2014.

[28] A. Mahmood and M. Chitre, "Viterbi detection of PSK signals in Markov impulsive noise," in *Proc. MTS/IEEE Kobe Techno-Oceans (OTO)*, 2018, pp. 1–6.

[29] G. Yang, J. Wang, W. Huang, G. Zhang, and S. Li, "CPFSK signals detection in bursty impulsive noise," in *Proc. IEEE Int. Conf. Commun. (ICC)*, 2019, pp. 1–6.

[30] D. Fertonani and G. Colavolpe, "On reliable communications over channels impaired by bursty impulse noise," *IEEE Trans. Commun.*, vol. 57, no. 7, pp. 2024–2030, Jul. 2009.

[31] M. S. Alam, B. Selim, I. Ahmed, G. Kaddoum, and H. Yanikomeroglu, "Bursty impulsive noise mitigation in NOMA: A MAP receiver-based approach," *IEEE Commun. Lett.*, vol. 25, no. 9, pp. 2790–2794, Sep. 2021.

[32] F. Sacuto, G. Ndo, F. Labeau, and B. L. Agba, "MAP optimum receiver mitigating correlated impulsive noise," in *Proc. IEEE Wireless Commun. Netw. Conf.*, 2016, pp. 1–6.

[33] D.-F. Tseng, F. G. Mengistu, Y. S. Han, M. Abera Mulatu, L.-C. Chang, and T.-R. Tsai, "Robust turbo decoding in a Markov Gaussian channel," *IEEE Wireless Commun. Lett.*, vol. 3, no. 6, pp. 633–636, Dec. 2014.

[34] G. Ndo, F. Labeau, and M. Kassouf, "A Markov-Middleton model for bursty impulsive noise: Modeling and receiver design," *IEEE Trans. Power Del.*, vol. 28, no. 4, pp. 2317–2325, Oct. 2013.

[35] H. Barka, M. S. Alam, G. Kaddoum, F. Sacuto, and B. L. Agba, "BNET: A neural network approach for LLR-based detection in the presence of bursty impulsive noise," *IEEE Wireless Commun. Lett.*, vol. 12, no. 1, pp. 80–84, Jan. 2023.

[36] B. L. Agba, F. Sacuto, M. Au, F. Labeau, and F. Gagnon, *Impulsive Noise Measurements*. Cham, Switzerland: Springer Int. Publ., 2019, pp. 119–138. [Online]. Available: https://doi.org/10.1007/978-3-319-91328-5_6

[37] L. Bahl, J. Cocke, F. Jelinek, and J. Raviv, "Optimal decoding of linear codes for minimizing symbol error rate (corresp.)," *IEEE Trans. Inf. Theory*, vol. 20, no. 2, pp. 284–287, Mar. 1974.

[38] F. Sacuto, F. Labeau, and B. L. Agba, "Fuzzy C-means algorithm for parameter estimation of partitioned Markov chain impulsive noise model," in *Proc. IEEE Int. Conf. Smart Grid Commun. (SmartGridComm)*, 2013, pp. 348–353.

[39] G. van der Nest, V. Lima Passos, M. J. Candel, and G. J. van Breukelen, "An overview of mixture modelling for latent evolutions in longitudinal data: Modelling approaches, fit statistics and software," *Adv. Life Course Res.*, vol. 43, Mar. 2020, Art. no. 100323. [Online]. Available: https://www.sciencedirect.com/science/article/pii/S1040260819301881

[40] T. K. Moon, "The expectation-maximization algorithm," *IEEE Signal Process. Mag.*, vol. 13, no. 6, pp. 47–60, Nov. 1996.

[41] J. Hoydis et al., "Sionna: An open-source library for next-generation physical layer research," 2023, *arXiv:2203.11854*.

[42] G. D. Forne, "The Viterbi algorithm," *Proc. IEEE*, vol. 61, no. 3, pp. 268–278, Mar. 1973.

HAZEM BARKA (Graduate Student Member, IEEE) received the B.Eng. degree in complex systems engineering from the Ecole Polytechnique de Tunisie, Université de Carthage, Tunisia. He is currently pursuing the Ph.D. degree in electrical engineering with the Ecole de Technologie Supérieure, Université du Québec, Montreal, Canada. His research focuses on developing advanced transceivers for smart grids to ensure robust and reliable communication under varying noise and fading conditions, particularly in the presence of bursty impulsive noise. His work emphasizes advanced impulsive noise modeling and mitigation techniques, leveraging AI and machine learning for symbol detection, multiple access techniques, semantic communication, and cooperative communication.

MD SAHABUL ALAM (Senior Member, IEEE) received the Ph.D. degree in electrical engineering from the Ecole de Technologie Superieure, Montreal, QC, Canada. He is currently an Assistant Professor with the Department of Electrical and Computer Engineering, California State University Northridge, Northridge, CA, USA. After finishing his Ph.D. degree, he worked as a Postdoctoral Fellow with the Systems and Computer Engineering Department, Carleton University, with the Prestigious Canadian Government FRQNT Fellowship. His current research interests include aerial communications with more focus on high altitude platform station-based communications, integration of terrestrial and non-terrestrial communications, reliable wireless communications in impulsive noise channels, cooperative communications, smart grid communications, NOMA, and massive MIMO for terrestrial and aerial communications. He was awarded the Governor General of Canada Gold Medal for Ph.D. degree.

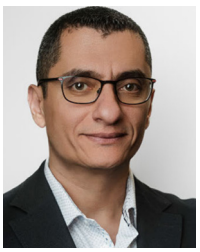

GEORGES KADDOUM (Senior Member, IEEE) received the bachelor's degree in electrical engineering from the École Nationale Supérieure de Techniques Avancées (ENSTA Bretagne), Brest, France, the M.S. degree in telecommunications and signal processing (circuits, systems, and signal processing) from the Université de Bretagne Occidentale and Telecom Bretagne (ENSTB), Brest, in 2005, and the Ph.D. degree (Hons.) in signal processing and telecommunications from the National Institute of Applied Sciences, University of Toulouse, Toulouse, France, in 2009. He is currently a Professor and the Research Director of the Resilient Machine Learning Institute, and the Tier 2 Canada Research Chair of the École de Technologie Supérieure (ÉTS), Université du Québec, Montreal, Canada. He has published more than 300 journal articles, conference papers, and two chapters in books, and has eight pending patents. His research interests include wireless communication networks, tactical communications, resource allocations, and network security. He received the Best Papers Award from the 2014 IEEE International Conference on Wireless and Mobile Computing, Networking, Communications, the 2017 IEEE International Symposium on Personal Indoor and Mobile Radio Communications, and the 2023 IEEE International Wireless Communications and Mobile Computing Conference . He received the IEEE Transactions on Communications Exemplary Reviewer Award in 2015, 2017, and 2019. He received the Research Excellence Award from the Université du Québec in 2018. In 2019, he received the Research Excellence Award from ÉTS in recognition of his outstanding research outcomes. He also won the 2022 IEEE Technical Committee on Scalable Computing Award for Excellence (Middle Career Researcher). He has received the prestigious 2023 MITACS Award for Exceptional Leadership. He served as an Associate Editor of IEEE TRANSACTIONS ON INFORMATION FORENSICS AND SECURITY and IEEE COMMUNICATIONS LETTERS. He is also serving as an Area Editor for IEEE TRANSACTIONS ON MACHINE LEARNING IN COMMUNICATIONS AND NETWORKING and an Editor for IEEE TRANSACTIONS ON COMMUNICATIONS.

MINH AU (Member, IEEE) received the B.Sc. and M.Sc. degrees in computer science and telecommunication from the University of Poitiers, Poitiers, France, in 2008 and 2010, respectively, and the Ph.D. degree in electrical engineering from the École de Technologie Supérieure, Montreal, QC, Canada, in 2016. He is actively involved in the Richard J. Marceau Industrial Research Chair for Wireless Internet in developing countries with Media 5 as a Postdoctoral Fellow. He is currently a Research Scientist with Hydro-Québec Research Institute, Varennes, QC, Canada. His current research interests include channel modeling in harsh and hostile environments, partial discharge phenomenon, low-latency communication for machine-to-machine, information theory on coding theory, and cybersecurity for smart grids.

BASILE L. AGBA (Senior Member, IEEE) received the M.Sc. and Ph.D. degrees in electronics and optoelectronics from the University of Limoges, Limoges, France, in 2001 and 2004, respectively. Since 2009, he has been an Adjunct Professor with the Electrical Engineering Department, École de Technologie Supérieure, Montreal, Canada. He is the Vision and Partnerships Manager and a Senior Scientist with Hydro-Quebec Research Institute. He is the coauthor of *Wireless Communications for Power Substations: RF Characterization and Modeling* (Springer). He has also authored more than 70 refereed papers in refereed journals and conference proceedings in these areas. He is an Active Member of International Telecommunication Union, Study Group 3 on radio propagation.